ChemPubSoc Europe

DOI: 10.1002/cctc.201500263

CHEMCATCHEM Full Papers

Synthesis and Peroxidase-Like Activity of Cobalt@Carbon-Dots Hybrid Material

Yali Guo, Xiaoyu Liu, Chengduan Yang, Xudong Wang, Dan Wang, Anam Iqbal, Weisheng Liu, and Wenwu Qin*[a]

A cobalt@carbon-dots (Co@C-dots) hybrid material is successfully prepared and well characterized. The hybrid material exhibits intrinsic peroxidase-like activity and can be utilized for the degradation of methylene blue; it shows enhanced catalytic activities compared with bare Co nanoparticles or C-dots. The good catalytic performance of the hybrid material may be attributed to synergistic effects between the Co nanoparticles and C-dots. Furthermore, the catalytic mechanism of the Co@C-dots hybrid material is also studied by using steady-state and time-resolved fluorometric analysis, which reveals that Co@C-dots can effectively decompose H_2O_2 to produce reactive hydroxyl radicals (•OH). These results suggest that the Co@C-dots hybrid material could be a promising material applied for biochemical analysis and water treatment.

Introduction

Peroxidases are a class of efficient biological catalysts and have been widely used in various fields, such as biotechnology, the chemical industry, and environmental science, among others.[1] However, these enzymes show many disadvantages, including the sensitivity of their catalytic activity to environmental conditions and the high costs in preparation and purification. Hence, much attention has been focused on developing novel peroxidase mimetics to replace the natural peroxidases. Gao et al. reported Fe_3O_4 nanoparticles (NPs) with an intrinsic enzyme mimetic activity, which is similar to that of natural peroxidases.[2] Subsequently, various nanomaterials, such as V_2O_5 nanowires,[3] CeO_2 NPs,[4] Co_3O_4 NPs,[5] MoS_2 nanosheets,[6] Au NPs,[7] metallic nanoalloys,[8,9] and carbon nanomaterials,[10,11] have also been reported to possess peroxidase-like catalytic activities. Compared with natural peroxidases, these peroxidase mimetics have the advantages of simple synthesis, design flexibility, and high catalytic activity. Peroxidase catalysis of the oxidation of organic dyes to reduce their toxicity is frequently used in wastewater treatment.[12] Organic dyes, such as methyl orange, methylene blue, rhodamine B, and methyl red, have detrimental effects on the environment or human body, and methods to degrade these toxic compounds are necessary for environmental protection.[13]

Recently, a variety of hybrid materials (graphene oxide–Fe_3O_4 magnetic nanocomposites,[14] $Au_{core}Pd_{shell}$–graphene hybrids,[15] Co_3O_4–reduced graphene oxide[16]) have been demonstrated to possess peroxidase-like catalytic activity. Hybrid materials, with well-defined structures, have been extensively explored to realize practical applications. The hybrid materials facilitate effective electron transfer and bring better catalytic performances than the corresponding single nanomaterials. Therefore, great efforts should be made to design and fabricate new hybrid materials with peroxidase-like activity.

Carbon dots (C-dots) are a new type of photoluminescent carbon nanomaterial and have attracted considerable attention as a result of their excellent photostability, good water solubility, favorable biocompatibility, and low toxicity.[17–20] In particular, the superb conductivity, rapid electron-transfer properties, and abundant oxygen-containing functionalized groups on the surface make C-dots much easier for forming environmentally friendly hybrid materials and can further enhance the catalytic activities of the original materials. Up to now, some groups have reported metal (Au,[21] Ag,[22] Pd,[23] Ni,[24] Cu,[25] and PtNi alloy[26]) nanoparticles@C-dots hybrid materials. The combination of metal NPs and C-dots provides a successful integration of the properties of the two components. In this contribution, we report the fabrication of a Co@C-dots hybrid material by a simple chemical reduction route. The morphology, structure, fluorescence properties, peroxidase-like activity, and catalytic mechanism of the hybrid material were systematically investigated.

Results and Discussion

1. Characterization of C-dots and Co@C-dots

The morphology and microstructure of C-dots and Co@C-dots are investigated by TEM. Figure 1 indicates that the prepared C-dots are spherical and well dispersed from each other. The particle size distribution obtained from dynamic light scatter-

[a] Y. Guo, X. Liu, C. Yang, X. Wang, D. Wang, A. Iqbal, Prof. W. Liu, Prof. W. Qin
Key Laboratory of Nonferrous Metal Chemistry and Resources Utilization of Gansu Province
Lanzhou University
Lanzhou, 730000 (P.R. China)
Fax: (+86) 931-8912582
E-mail: qinww@lzu.edu.cn

Supporting Information for this article is available on the WWW under http://dx.doi.org/10.1002/cctc.201500263.

© 2015 Wiley-VCH Verlag GmbH & Co. KGaA, Weinheim

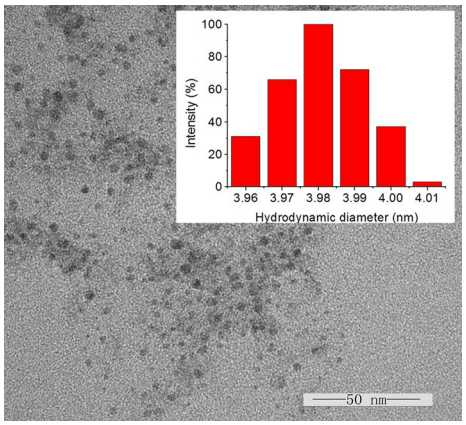

Figure 1. TEM image of as-prepared C-dots. (Inset: Size distribution histogram obtained from dynamic light scattering measurements.)

ing measurements shows that the average hydrodynamic diameter of the C-dots is approximately 4.0 nm (inset of Figure 1). Figure 2 shows TEM images of the Co@C-dots with core–shell nanostructures. An ultrathin continuous C-dots layer covers the Co NP surface. The Co NPs appear to form chainlike structures embedded within a carbon matrix, which suggests that the deposition of the Co NPs is initiated from the carbon particle surface.[25] The high-resolution TEM image also demonstrates that the Co cores are coated with ultrathin C-dot shells (Figure 2c). Notably, the Co cores consist of much smaller NPs, and this type of structure can further improve the catalytic activity of the Co@C-dots as a result of the increased surface area and catalytic active sites. Figure 2d shows the corresponding energy-dispersive X-ray (EDX) spectroscopy image of the hybrid material. The result confirms the presence of the Co element in the hybrid material. Moreover, the intensity of the carbon signal with Co@C-dots is stronger than the background (Figure S1 in the Supporting Information). To evaluate the composition and elemental distribution of the hybrid material, EDX elemental-mapping analysis is performed, and the results reveal that the elements C, O, and Co are present in the hybrid material (Figure 3).

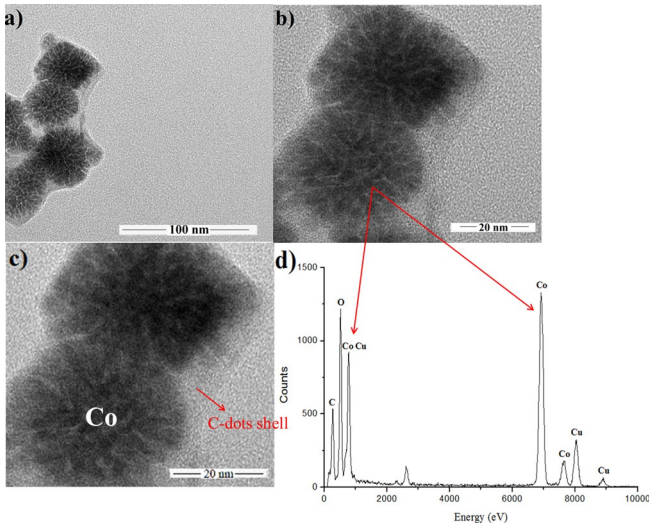

Figure 2. a, b) TEM images of Co@C-dots with different magnifications. c) HRTEM image of Co@C-dots nanoparticles. d) EDX pattern of Co@C-dots.

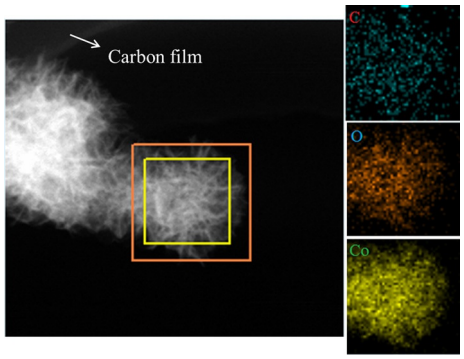

Figure 3. High-angle annular dark-field TEM image and mapping results of the elements C, O, and Co for the boxed area.

The formation mechanism of the Co@C-dots hybrid material is proposed. If the cobalt salt is mixed with a C-dot suspension, some Co^{2+} ions get attached to the surface of the C-dots by ion exchange or electrostatic interactions. Upon addition of the reducing agent, the Co^{2+} ions are reduced in situ to Co atoms, which serve as the nucleation seeds for the growth of small Co NPs. The strong magnetic interactions among the small Co NPs then make the agglomerates into larger quasi-spherical nanoparticles. At the same time, the C-dots form a thin layer around the Co NP surface.

The XRD pattern of the as-prepared Co@C-dots is displayed in Figure S2 in the Supporting Information. It has no obvious peak for cobalt and implies that the sample is almost in an amorphous state.[29] Relative to the crystalline state, this type of amorphous structure has been reported to possess many more catalytic active sites.[30] The result is in good agreement with the TEM results.

The surface chemical compositions and the valence states of the Co@C-dots are determined by XPS analysis. The existence of C (C 1s), O (O 1s), and Co (Co 2p) elements in the spectrum suggests the formation of the Co@C-dots hybrid material (Figure 4a).[31] Figure 4b is a typical Co 2p spectrum of the Co@C-dots, which indicates the hybrid consists of zero-valence cobalt and cobalt oxide; the result may be caused by surface oxidation during the sample preparation process for XPS measurements.[29]

Moreover, we further investigate the interactions between the C-dot and Co NP components in the hybrid material. The FTIR spectra of C-dots and Co@C-dots are shown in Figure S3 in the Supporting Information. The FTIR spectrum of the C-dots exhibits characteristic absorption bands of O–H at $\tilde{\nu}=$ 3425 cm^{-1}, C=O at $\tilde{\nu}=1758\ cm^{-1}$, COO^- at $\tilde{\nu}=1572\ cm^{-1}$, and C–H at $\tilde{\nu}=1388\ cm^{-1}$, respectively. Relative to the spectra for the C-dots, the C=O stretching peaks ($\tilde{\nu}=1758\ cm^{-1}$) have disappeared for the Co@C-dots, and the COO^- asymmetric stretching vibration peak ($\tilde{\nu}=1572\ cm^{-1}$) of the Co@C-dots is also decreased and shifted if they are involved in Co NP forma-

© 2015 Wiley-VCH Verlag GmbH & Co. KGaA, Weinheim

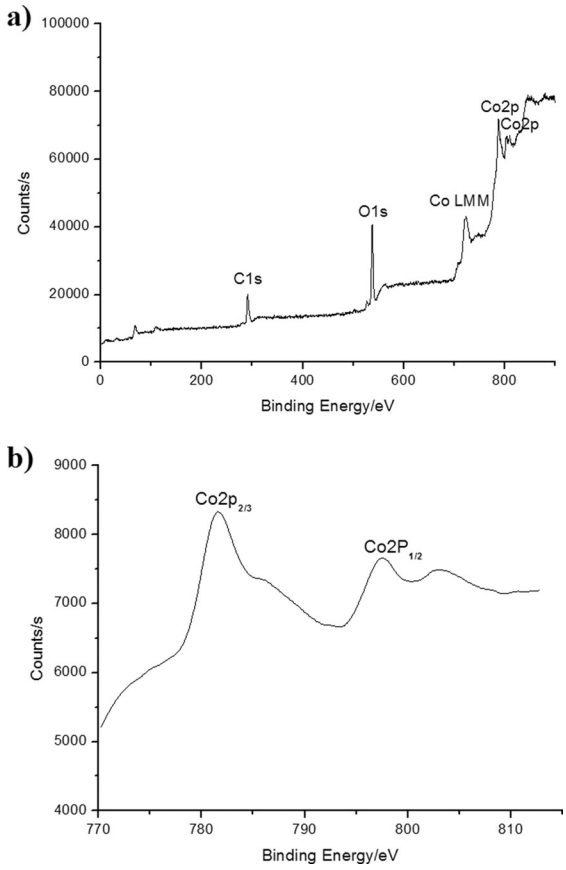

Figure 4. XPS spectra of a) Co@C-dots and b) Co 2p.

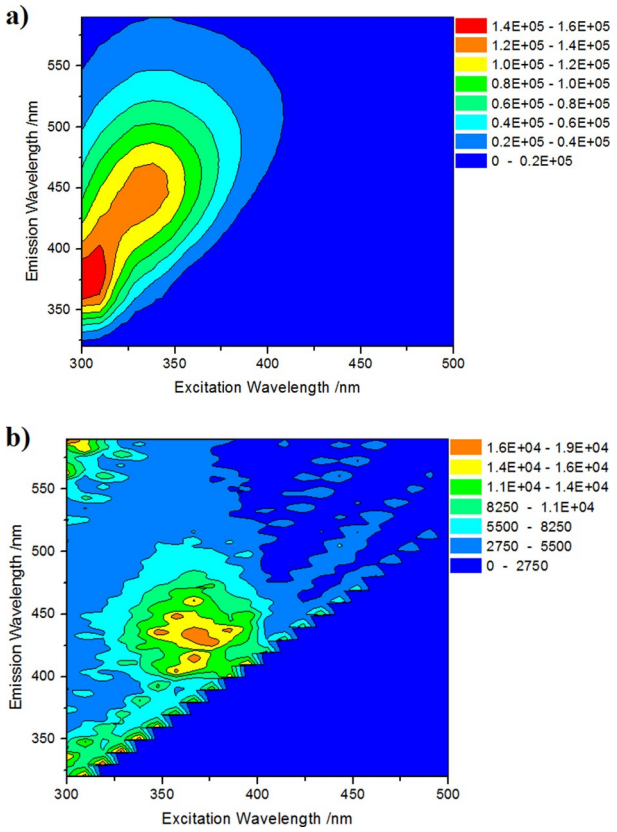

Figure 5. 3D excitation–emission intensity maps of a) C-dots and b) Co@C-dots dispersed in double-distilled water.

tion, which may be attributed to the bonding interactions between the carboxylate groups and the metal.[24,25]

2. Fluorescence properties

To gain further insight into the interaction between the Co NPs and C-dots, we collected the 3D and 2D photoluminescence spectra of both C-dots and Co@C-dots (Figure 5 and Figure S4 and S5 in the Supporting Information). The fluorescence emission spectra and photoluminescence intensity of the C-dots depend on the changes of excitation wavelength, which are similar to the reports in the literature.[32–34] The maximum intensity region of the C-dots appears in the $\lambda = 320$–360 nm range for excitation and the $\lambda = 420$–460 nm range for emission.[35] The formation of the Co@C-dots quenches remarkably the photoluminescence of the C-dots (Figure 5b and Figure S5 in the Supporting Information). The quantum yield of the Co@C-dots (0.4%) is also much lower than that of the C-dots (7.6%). We consider that the electron may transfer between the C-dot shells and the Co cores; therefore, the formation of the Co@C-dots quenches remarkably the photoluminescence of the C-dots. This kind of quenching phenomenon has also been observed in the other metal-NP@C-dots systems.[21–26]

The fluorescence decay of both C-dots and Co@C-dots was also investigated through the single-photon timing technique (Figure 6, Table S1 and Figure S6–S8 in the Supporting Information). The fluorescence decay of the C-dots in water displays biexponential behavior, and the biexponential function ($\tau \approx 1.8$ and ≈ 6.1 ns) is used to fit the decays at all three emission wavelengths. Additionally, the different emission wavelengths of the C-dots do not induce an obvious change in the fluorescence decay, and the decay times are similar to those reported in the literature.[24]

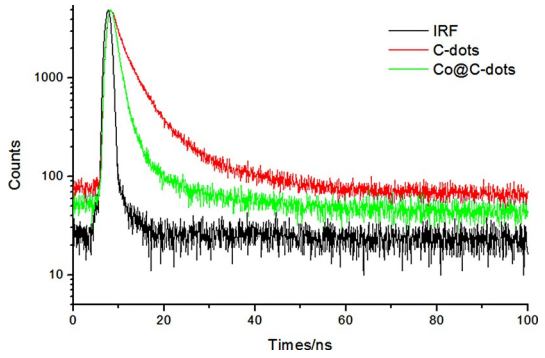

Figure 6. Fluorescence decay profiles ($\lambda_{ex} = 300$ nm and $\lambda_{em} = 460$ nm) of C-dots and Co@C-dots aqueous suspension.

The fluorescence decay for the Co@C-dots also reveals a biexponential behavior, and the shorter lifetime decreased (from $\tau \approx 1.8$ to ≈ 1.1 ns) along with an increase in the amplitude (from ≈ 42 to $\approx 85\%$). The longer component remained almost constant (between $\tau \approx 6.1$ to ≈ 6.2 ns), and the contri-

© 2015 Wiley-VCH Verlag GmbH & Co. KGaA, Weinheim

bution of this component decreased (from ≈58 to ≈15%). Figure 6 shows that the fluorescence lifetimes of the Co@C-dots decrease (become shorter) relative to those of the C-dots. The photoexcited C-dots can serve as both electron donors and electron acceptors,[22] and the Co NPs core can also provide free electrons. The electron is transferred between the C-dots and Co NP cores and can further quench the excited state of the C-dots; hence, the fluorescence lifetimes of the Co@C-dots become shorter than those the C-dots. The different fluorescence properties between the C-dots and Co@C-dots further confirm that the Co@C-dots hybrid material is successfully prepared.

3. Peroxidase-like activity of Co@C-dots

The peroxidase-like activity of the Co@C-dots is tested for the catalytic oxidation of 3,3′,5,5′-tetramethylbenzidine (TMB) in the presence of H_2O_2. As shown in Figure 7, the Co@C-dots can catalyze the oxidation of TMB, with H_2O_2 employed as the oxidant, to produce a blue-colored solution, which suggests that the Co@C-dots possess peroxidase-like catalytic activity. The maximum absorbance of the reaction system is $\lambda =$ 652 nm, which originates from the oxidation of TMB.[36,37] Moreover, we further examined the effects of pH value, temperature, and concentration of H_2O_2 on the catalytic activity of both the Co@C-dots and natural horseradish peroxidase (HRP; see Section 1.3 in the Supporting Information). The experimental results show that the optimal reaction conditions for the Co@C-dots are pH 3.0, $T = 45\,^{\circ}C$, and 25 mM H_2O_2. The catalytic activity of the Co@C-dots, similar to that of HRP, is higher in an acidic medium than in a neutral medium (Figure 8a).[38] Notably, the Co@C-dots hybrid material exhibits an improved thermal stability over that of HRP. The HRP starts to lose its activity above $T = 30\,^{\circ}C$, whereas the Co@C-dots still have high activity at $T = 60\,^{\circ}C$ (Figure 8b). In addition, the catalytic activity of the hybrid material is inhibited at high H_2O_2 concentrations (Figure 8c). This behavior is similar to that of other NP-based peroxidase mimetics[39,40] and further confirms the peroxidase-like activity of the Co@C-dots. Additionally, control experiments show that the absorbance of the Co@C-dots/TMB/H_2O_2 system at $\lambda = 652$ nm is higher than the bare Co NP or C-dot systems (Figure 8d), which is probably due to synergistic effects between the Co NPs[8] (Figure S9 and Section 1.2 in the Supporting Information) and the C-dots.[24]

Steady-state kinetic experiments are performed to investigate further the peroxidase-like activity of the Co@C-dots. A series of experiments are performed by changing the concen-

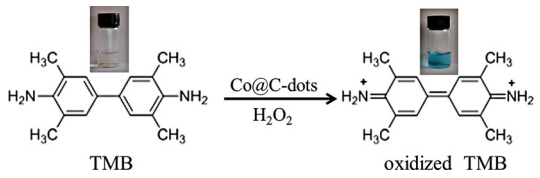

Figure 7. The Co@C-dots/TMB/H_2O_2 system.

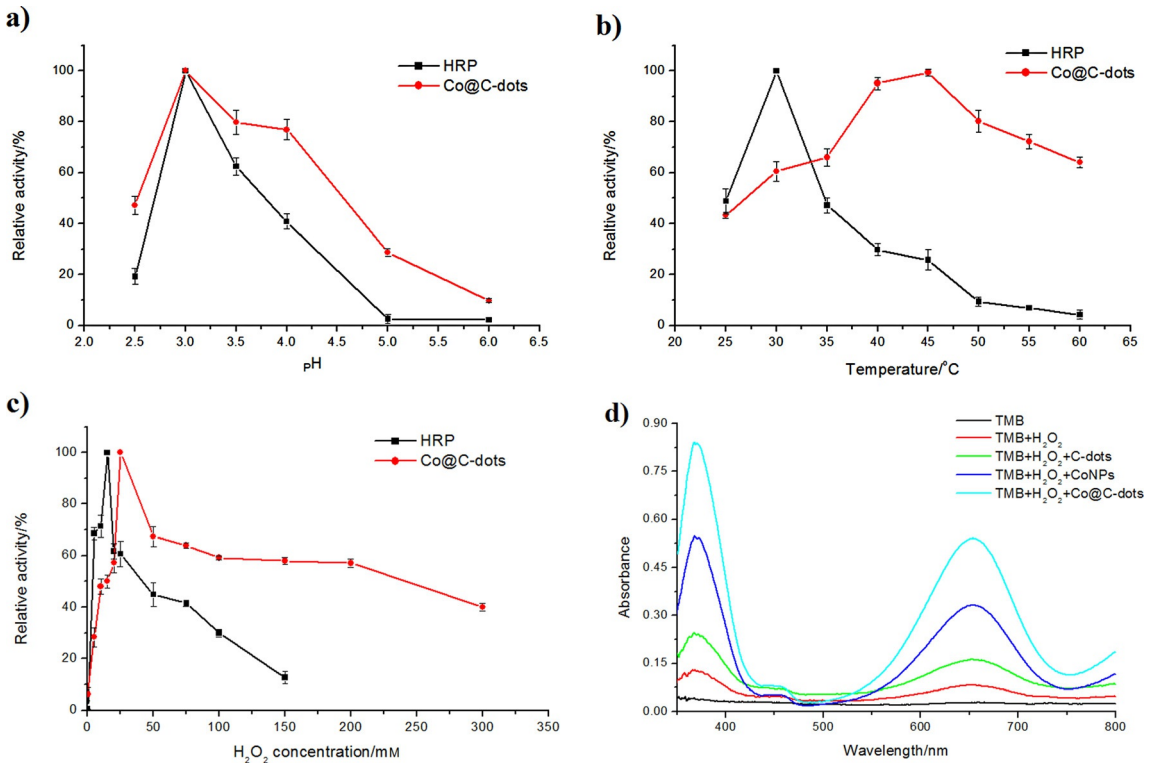

Figure 8. Dependence of the catalytic activity of HRP (black curve) and Co@C-dots (red curve) on a) pH value, b) temperature, and c) H_2O_2 concentration ($T = 45\,^{\circ}C$ for Co@C-dots, $T = 30\,^{\circ}C$ for HRP). The maximum point in each curve was set as 100%. Error bars represent the standard error derived from three repeated measurements. d) The UV/Vis absorption spectra of TMB in different reaction systems under the optimal reaction conditions.

© 2015 Wiley-VCH Verlag GmbH & Co. KGaA, Weinheim

tration of TMB and H_2O_2, respectively. In a certain range of substrate concentrations, typical Michaelis–Menten curves can be obtained, as shown in Figure 9. The maximum initial velocity (V_m) and Michaelis–Menten constant (K_m) are calculated from the Lineweaver–Burk plots (Table S2 and Figure S10 in the Supporting Information). The K_m value is an important parameter used to measure the binding affinity of the enzyme for the substrate and can also be used to study the enzyme mimetic–substrate interaction. The apparent value for the Co@C-dots with TMB is $K_m = 0.32$ mM, which is lower than that of HRP ($K_m = 0.43$ mM).[2] The result indicates that the Co@C-dots have a higher affinity for TMB than the natural enzyme HRP. In contrast, the K_m value of Co@C-dots with H_2O_2 as the substrate ($K_m = 4.81$ mM) is higher than that of HRP ($K_m = 3.7$ mM), which indicates that the Co@C-dots have a lower affinity for H_2O_2 than HRP. The result is consistent with the observation that a higher H_2O_2 concentration is needed with the Co@C-dots than with HRP if the maximum activity is to be obtained.

The Co@C-dots hybrid material is also tested as a peroxidase mimetic for the catalytic oxidation of methylene blue (MB; see Section 1.4 and Figure S11 and S12 in the Supporting Information). The results reveal that the catalytic efficiency of the Co@C-dots is more effective than bare Co NPs or C-dots, which indicates that the Co@C-dots have high catalytic degradation activity. No obvious decolorization is observed in the absence of catalyst, which demonstrates that the degradation of MB is caused by catalytic oxidation of H_2O_2.

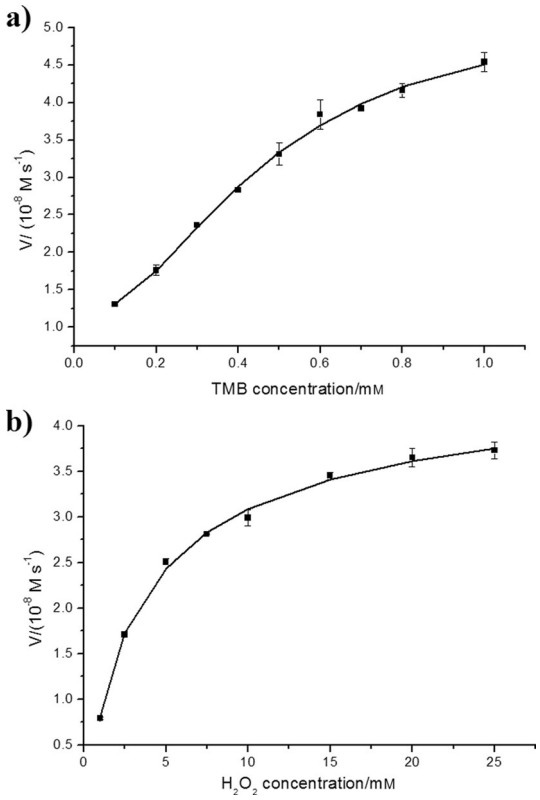

Figure 9. Steady-state kinetic assays of the Co@C-dots. a) The concentration of H_2O_2 was 100 mM and the TMB concentration was varied. b) The concentration of TMB was 8 mM and the H_2O_2 concentration was varied. Error bars represent the standard error derived from three repeated measurements.

4. Mechanism of peroxidase-like activity of Co@C-dots

To demonstrate the peroxidase-like catalytic mechanism of the Co@C-dots, we study the steady-state fluorescence changes of terephthalic acid (TA) in the presence of H_2O_2 and the Co@C-dots. TA is a highly sensitive and selective fluorescent probe for hydroxyl radicals (•OH). The weakly fluorescent TA can react with •OH and convert into the highly fluorescent 2-hydroxyterephthalic acid (HTA). Figure 10b displays the photoluminescence spectra of a TA/H_2O_2 system with different volumes of Co@C-dots. The photoluminescence spectrum of the TA/H_2O_2/Co@C-dots system is similar to that of HTA (Figure 10a), and the fluorescence intensity of the solution increases with the addition of Co@C-dots. The fluorescence intensity of the TA/H_2O_2/Co@C-dots system has a linear relationship within a certain concentration range of Co@C-dots (Figure S13 in the Supporting Information). In addition, contrast experiments were performed with C-dots and Co NPs (Figure S14 in the Supporting Information). The results show that the fluorescence intensity of the TA/H_2O_2/Co@C-dots system is stronger than that of bare Co NP or C-dot systems under the same conditions, which indicates that the Co@C-dots can catalyze the decomposition of hydrogen peroxide to produce more hydroxyl radicals. The above results suggest that the Co@C-dots can effectively catalyze the decomposition of H_2O_2 to •OH.

Most mechanism studies of peroxidase-like activity focus on the steady-state fluorescence changes of TA,[41–42] and the time-resolved fluorescence has not been studied before. The gener-

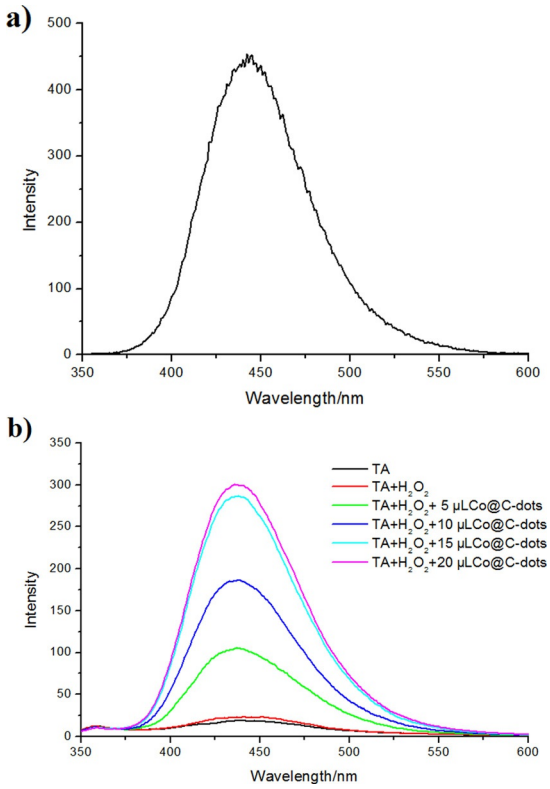

Figure 10. a) Photoluminescence spectrum of HTA. b) Emission spectra of TA in the presence of H_2O_2 and different volumes of Co@C-dots.

© 2015 Wiley-VCH Verlag GmbH & Co. KGaA, Weinheim

Table 1. Photophysical properties of HTA, HTA + TA, HTA/H_2O_2/Co@C-dots, and TA/H_2O_2/Co@C-dots systems. Decay times τ_1 and τ_2 and the relative amplitude are given.

System	Excitation wavelength [nm]	Emission wavelength [nm]	τ_1 [ns] (amplitude [%])	τ_2 [ns] (amplitude [%])
TA/H_2O_2/Co@C-dots	300	440	1.78 (17.5)	9.20 (82.4)
HTA	300	440	9.91 (100)	–
TA + HTA	300	440	1.97 (5.29)	9.57 (94.7)
HTA/H_2O_2/Co@C-dots	300	440	9.47 (100)	–

ated highly fluorescent HTA can be employed to study the catalytic mechanism of the Co@C-dots by time-resolved fluorescence analysis. Based on the above discussion, we further study the fluorescence decay of the HTA, TA + HTA, HTA/H_2O_2/Co@C-dots, and TA/H_2O_2/Co@C-dots systems (Table 1 and Figure 11). The fluorescence decay of neat HTA in water at $\lambda_{ex} = 300$ nm displays monoexponential behavior ($\tau \approx 9.9$ ns). When the HTA (95%) is mixed with a small amount of TA (5%) in aqueous solution, the result shows biexponential behavior ($\tau \approx 2.0$ and ≈ 9.6 ns), and we consider that the two components are derived from TA ($\tau \approx 2.0$ ns) and HTA ($\tau \approx 9.6$ ns; Table 1). The fluorescence decay of the TA/H_2O_2/Co@C-dots system is fitted to the biexponential profile with lifetimes of $\tau \approx 1.8$ and 9.2 ns. The slow decay may be attributed to the lifetime of HTA (TA reacts with $^{\bullet}OH$) molecules, whereas the fast decay may be attributed to the lifetime of the remaining TA. The lifetime of the Co@C-dots cannot be found here, which is attributed to the small amount of Co@C-dots in the reaction system. Notably, the fluorescence lifetimes of the TA/H_2O_2/Co@C-dots ($\tau \approx 9.2$ ns) and HTA/H_2O_2/Co@C-dots ($\tau \approx 9.5$ ns) systems become shorter than that of neat HTA ($\tau \approx 9.9$ ns). This phenomenon may a result of the formation of $^{\bullet}OH$ in those systems, because the extra free radical/electron can further partly quench the excited state of HTA (Table 1). The time-resolved fluorescence data further confirm that the Co@C-dots can catalyze decomposition of H_2O_2 to $^{\bullet}OH$.

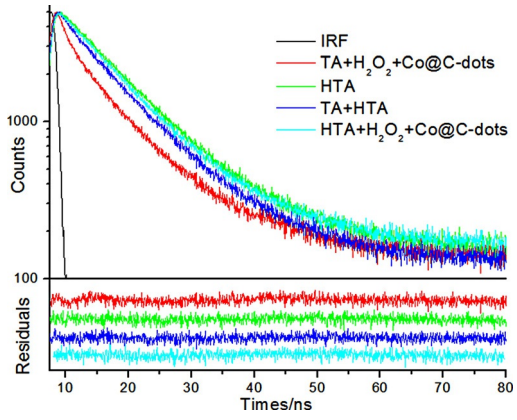

Figure 11. Fluorescence decay profiles and residuals of HTA, TA + HTA, HTA/H_2O_2/Co@C-dots, and TA/H_2O_2/Co@C-dots systems with excitation at $\lambda = 300$ nm.

On the basis of the results and discussions presented above, a plausible catalytic mechanism for the Co@C-dots is proposed (Scheme 1). Firstly, the H_2O_2 adsorbs on the Co@C-dots surface, and the Co@C-dots can decompose the H_2O_2 into $^{\bullet}OH$ radicals. Subsequently, the good electron-transport properties of the C-dot shell facilitate the electron transfer from the $^{\bullet}OH$ radical to the reaction substrate (TMB or MB), and the substrates can be easily oxidized by the $^{\bullet}OH$ radicals. For bare Co NPs, there is no electronic transmission medium to accelerate the electron transfer. Hence, the reaction rate drops to a lower level relative to that of the Co@C-dots.

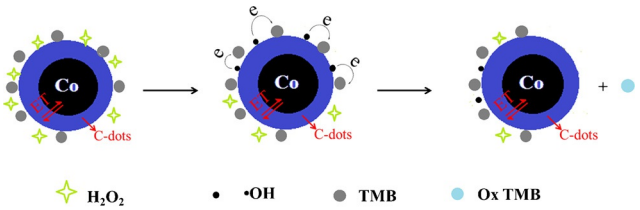

Scheme 1. Possible mechanism for theCo@C-dots/H_2O_2/TMB system.

Conclusions

In summary, a Co@C-dots hybrid material has been successfully prepared by a simple chemical reduction route. The morphology, structure, and fluorescence properties of the hybrid material are studied. Further catalytic experiments demonstrate that the Co@C-dots material possesses intrinsic peroxidase-like activity and its catalytic activity is affected by the pH value, the temperature, and the concentration of H_2O_2. In addition, the obtained Co@C-dots hybrid material exhibits enhanced catalytic activity for the degradation of methylene blue. The catalytic mechanism of the Co@C-dots is further investigated by means of steady-state and time-resolved fluorometry analyses, which show that the Co@C-dots can effectively decompose H_2O_2 to produce reactive hydroxyl radicals ($^{\bullet}OH$). The results suggest that the Co@C-dots hybrid material can be a promising material for a wide range of potential applications in biochemical analysis and water treatment.

Experimental Section

Chemicals

Cobalt(II) chloride ($CoCl_2 \cdot 6H_2O$; Beijing Chemical Works; ≥99%), sodium borohydride ($NaBH_4$; ≥96%), and hydrogen peroxide (H_2O_2; ≥30 wt%) were purchased from Sinopharm Chem. Reagent Co., Ltd. Citric acid monohydrate (≥99.5%), sodium hydroxide (NaOH; ≥96%), hydrazine monohydrate ($H_2NNH_2 \cdot H_2O$; ≥80%), and ethylene glycol ($HOCH_2CH_2OH$) were purchased from Tianjin

© 2015 Wiley-VCH Verlag GmbH & Co. KGaA, Weinheim

Guangfu Reagent Company. 3,3′,5,5′-tetramethylbenzidine (TMB; ≥98%), horseradish peroxidase (HRP; 250 U mg^{-1}), and 2-hydroxyterephthalic acid (HTA; 98%) were purchased from Energy Chemical. Terephthalic acid (TA; ≥98.5%) and methylene blue (MB; ≥98.5%) were purchased from Chengdu cologne chemical reagent factory. All reagents and solvents were of analytical grade and used directly without further purification, and all aqueous solutions were prepared with Milli-Q water (18.2 MΩ cm).

Instruments

The morphology and microstructure of samples were analyzed by transmission electron microscopy (TEM) on a JEM-2100 instrument equipped with an energy-dispersive X-ray (EDX) spectrometer. The samples were dispersed in ethanol and then dried on a micro grid. X-ray diffraction (XRD) measurements were performed on an X-ray diffractometer (D/max-2400pc, Rigaku, Japan) with $Cu_{K\alpha}$ radiation ($\lambda = 1.54178$ Å), by using an operating voltage and current of 40 kV and 60 mA, respectively. The 2θ range was from 10° to 90° in steps of 0.02°. For XRD observations, the samples were dispersed in ethanol and then dried on a glass slide. X-ray photoelectron spectra (XPS) were measured on a PHI-550 spectrometer by using $Mg_{K\alpha}$ radiation ($h\nu = 1253.6$ eV) with a base vacuum operated at 300 W. The Fourier transform infrared (FTIR) spectra were measured on a Nicolet 360 FTIR spectrometer by using the KBr pellet technique.

Steady-state UV/Vis absorption and fluorescence spectroscopy

The absorbances of catalytic reaction processes were recorded on a UV/visible spectrometer (Cary 100) under experimental conditions. The steady-state excitation and emission spectra were obtained on an FLS920 spectrofluorometer. 3D maps were collected with an excitation range of $\lambda = 300$–500 nm and an emission range of $\lambda = 320$–590 nm. Freshly prepared samples in 1 cm quartz cells were used to perform all UV/Vis absorption and emission measurements.

Quantum yields were determined by an absolute method with an integrating sphere based upon that originally developed by de Mello[27] et al. Experiments were conducted on an FLS920 spectrofluorometer from Edinburgh Instruments.

Time-resolved fluorescence spectroscopy

Fluorescence lifetimes were measured on an Edinburgh Instruments FLS920 spectrofluorometer equipped with different light-emitting diodes (excitation wavelengths of $\lambda = 300$ and 330 nm), by using the time-correlated single-photon counting technique[28] in 2048 channels at room temperature. The sample concentrations were adjusted to optical densities of <0.1 at the excitation wavelength ($\lambda = 300$ or 330 nm). The monitored wavelengths were $\lambda =$ 440, 460, and 480 nm.

Histograms of the instrument response functions (by using LUDOX scattering) and sample decays were recorded until they reached typically 5.0×103 counts in the peak channel. The obtained histograms were fitted as sums of the exponentials, with Gaussian-weighted nonlinear least squares fitting based on the Marquardt–Levenberg minimization implemented in the software package of the instrument. The fitting parameters (decay times and pre-exponential factors) were determined by minimizing the reduced chi-square, χ^2. An additional graphical method was used to judge the quality of the fit that included plots of surfaces ("carpets") of the weighted residuals versus the channel number. All curve fittings presented here had minimizing the reduced chi-square, χ^2, values of <1.1.

Synthesis of Co@C-dots

C-dots were prepared according to our previous report, and the details are described in Section 1.1 of the Supporting Information.[24] The Co@C-dots hybrid material was prepared by a simple chemical reduction route. Typically, an amount of cobalt chloride (1.07 g) was dissolved directly in ethylene glycol (100 mL), and $CoCl_2{\cdot}6H_2O$ solution (45 mM; 10 mL) was mixed with an aqueous suspension of C-dots (10 mL) in a 100 mL round-bottom flask with a magnetic stirrer bar. After the mixture had been stirred for a few minutes, hydrazine hydrate (1.125 g) was then added to the above solution. The mixture was kept vigorously stirring at $T = 60$ °C for 30 min. Subsequently, a 5 mg mL^{-1} $NaBH_4$ aqueous solution was added dropwise to trigger the reaction. The bright-red solution became dark, which indicated the formation of Co NPs, and was kept stirring for another 1 h at $T = 60$ °C. Finally, the product was washed with absolute alcohol and dissolved as an aqueous solution (5 mg mL^{-1}) to generate a colloidal suspension of Co@C-dots nanoparticles.

Peroxidase-like activity of the Co@C-dots

The peroxidase-like activity of the Co@C-dots hybrid material was tested through the catalytic oxidation of the peroxidase substrate 3,3′,5,5′-tetramethylbenzidine (TMB) in the presence of H_2O_2. Typically, TMB (8 mM; 50 μL), H_2O_2 (30 wt%; 20 μL), and colloidal Co@C-dots nanoparticles (50 μL) were added into sodium acetate buffer solution (2 mL; pH 3.0) at $T = 45$ °C, unless otherwise stated. The reactions were carried out for 10 min and then were monitored by observing the absorbance at $\lambda = 652$ nm. The relative activity was calculated by A_1/A_2, in which A_2 was the maximum absorbance and A_1 was the sample absorbance measured under the same conditions.

Kinetic analysis

The kinetic analysis was carried out by monitoring the absorbance at various times with a spectrophotometer. The experiments were performed at $T = 45$ °C with enzyme mimetics (5 mg L^{-1}; 50 μL) in a 2 mL reaction volume of sodium acetate buffer solution (pH 3.0) with 8 mM TMB or 100 mM H_2O_2 as a substrate, unless otherwise stated. The Michaelis–Menten constant was calculated by using the Lineweaver–Burk plot: $1/V_0 = (K_m/V_m)(1/[S] + 1/K_m)$, in which V_0 is the initial velocity, V_m is the maximal reaction velocity, and [S] is the concentration of the substrate.

The measurement of the hydroxyl free radicals

The reaction was performed in a TA solution (1 mM; 2 mL) with H_2O_2 (30 wt%; 6 μL) and different volumes of Co@C-dots. The fluorescence spectrum was then measured between $\lambda = 350$ and 600 nm with $\lambda = 315$ nm as the excitation wavelength. The same experiments were also performed for C-dots and Co NPs.

© 2015 Wiley-VCH Verlag GmbH & Co. KGaA, Weinheim

Acknowledgements

This work was supported by the National Science Foundation for Fostering Talents in Basic Research of the National Natural Science Foundation of China (grant no. J1103307).The authors would like to thank the Natural Science Foundation of China (no. 21271094).

Keywords: carbon · cobalt · fluorescence · hybrid materials · radical reactions

[1] A. X. Zheng, Z. X. Cong, J. R. Wang, J. Li, H. H. Yang, G. N. Chen, *Biosens. Bioelectron.* **2013**, *49*, 519 – 524.
[2] L. Gao, J. Zhuang, L. Nie, J. Zhang, Y. Zhang, N. Gu, T. Wang, J. Feng, D. Yang, S. Perrett, *Nat. Nanotechnol.* **2007**, *2*, 577 – 583.
[3] R. André, F. Natálio, M. Humanes, J. Leppin, K. Heinze, R. Wever, H. C. Schröder, W. G. Müller, W. Tremel, *Adv. Funct. Mater.* **2011**, *21*, 501 – 509.
[4] T. Pirmohamed, J. M. Dowding, S. Singh, B. Wasserman, E. Heckert, A. S. Karakoti, J. E. S. King, S. Seal, W. T. Self, *Chem. Commun.* **2010**, *46*, 2736 – 2738.
[5] J. F. Yin, H. Q. Cao, Y. X. Lu, *J. Mater. Chem.* **2012**, *22*, 527 – 534.
[6] T. R. Lin, L. S. Zhong, L. Q. Guo, F. F. Fu, G. N. Chen, *Nanoscale* **2014**, *6*, 11856 – 11862.
[7] Y. Jv, B. X. Li, R. Cao, *Chem. Commun.* **2010**, *46*, 8017 – 8019.
[8] Y. J. Chen, H. Y. Cao, W. B. Shi, H. Liu, Y. M. Huang, *Chem. Commun.* **2013**, *49*, 5013 – 5015.
[9] W. W. He, Y. Liu, J. S. Yuan, J. J. Yin, X. C. Wu, X. N. Hu, K. Zhang, J. B. Liu, C. Y. Chen, Y. L. Ji, Y. T. Guo, *Biomaterials* **2011**, *32*, 1139 – 114.
[10] W. B. Shi, Q. L. Wang, W. J. Long, Z. L. Cheng, S. H. Chen, H. Z. Zheng, Y. M. Huang, *Chem. Commun.* **2011**, *47*, 6695 – 6697.
[11] Y. J. Song, K. G. Qu, C. Zhao, J. S. Ren, X. G. Qu, *Adv. Mater.* **2010**, *22*, 2206 – 2210.
[12] A. Bhunia, S. Durani, P. P. Wangikar, *Biotechnol. Bioeng.* **2001**, *72*, 562 – 567.
[13] M. Kumar, S. Deka, *ACS Appl. Mater. Interfaces* **2014**, *6*, 16071 – 16081.
[14] Y. L. Dong, H. G. Zhang, Z. U. Rahman, L. Su, X. J. Chen, J. Hu, X. G. Chen, *Nanoscale* **2012**, *4*, 3969 – 3976.
[15] X. Y. Chen, Y. Li, F. B. Zhang, G. L. Zhang, X. B. Fan, *J. Mater. Chem.* **2011**, *21*, 17658 – 17661.
[16] J. X. Xie, H. Y. Cao, H. Jiang, Y. J. Chen, W. B. Shi, H. Z. Zheng, Y. M. Huang, *Anal. Chim. Acta* **2013**, *796*, 92 – 100.
[17] H. T. Li, X. D. He, Z. H. Kang, Y. Liu, J. L. Liu, S. Y. Lian, C. H. A. Tsang, X. B. Yang, S.-T. Lee, *Angew. Chem. Int. Ed.* **2010**, *49*, 4430 – 4434; *Angew. Chem.* **2010**, *122*, 4532 – 4536.
[18] S. N. Baker, G. A. Baker, *Angew. Chem. Int. Ed.* **2010**, *49*, 6726 – 6744; *Angew. Chem.* **2010**, *122*, 6876 – 6896.
[19] Y. P. Sun, B. Zhou, Y. Lin, W. Wang, K. A. Shiral Fernando, P. Pathak, M. J. Meziani, B. A. Harruff, X. Wang, H. F. Wang, P. G. Luo, H. Yang, M. E. Kose, B. L. Chen, L. M. Veca, S. Y. Xie, *J. Am. Chem. Soc.* **2006**, *128*, 7756 – 7757.
[20] X. D. Wang, D. Wang, Y. L. Guo, C. D. Yang, A. Iqbal, W. S. Liu, W. W. Qin, D. Yan, H. C. Guo, *Dalton Trans.* **2015**, *44*, 5547 – 5554.
[21] P. H. Luo, C. Li, G. Q. Shi, *Phys. Chem. Chem. Phys.* **2012**, *14*, 7360 – 7366.
[22] L. M. Shen, M. L. Chen, L. L. Hu, X. W. Chen, J. H. Wang, *Langmuir* **2013**, *29*, 16135 – 16140.
[23] D. Dey, T. Bhattacharya, B. Majumdar, S. Mandani, B. Sharma, T. K. Sarma, *Dalton Trans.* **2013**, *42*, 13821 – 13825.
[24] Y. L. Guo, D. Wang, X. Y. Liu, X. D. Wang, W. S. Liu, W. W. Qin, *New J. Chem.* **2014**, *38*, 5861 – 5867.
[25] L. Tian, D. Ghosh, W. Chen, S. Pradhan, X. J. Chang, S. W. Chen, *Chem. Mater.* **2009**, *21*, 2803 – 2809.
[26] J. K. Sun, Q. Xu, *ChemCatChem* **2015**, *7*, 526 – 631.
[27] J. C. de Mello, H. F. Wittmann, R. H. Friend, *Adv. Mater.* **1997**, *9*, 230 – 232.
[28] N. Boens, W. W. Qin, N. Basaric, J. Hofkens, M. Ameloot, *Anal. Chem.* **2007**, *79*, 2137 – 2149.
[29] L. Yang, N. Cao, C. Du, H. M. Dai, K. Hu, W. Luo, G. Z. Cheng, *Mater. Lett.* **2014**, *115*, 113 – 116.
[30] J. M. Yan, X. B. Zhang, H. Shioyama, Q. Xu, *J. Power Sources* **2010**, *195*, 1091 – 1094.
[31] D. Wang, Y. L. Guo, W. S. Liu, W. W. Qin, *RSC Adv.* **2014**, *4*, 7435 – 7439.
[32] X. F. Jia, J. Li, E. K. Wang, *Nanoscale* **2012**, *4*, 5572 – 5575.
[33] Z. Lin, W. Xue, H. Chen, J. Lin, *Anal. Chem.* **2011**, *83*, 8245 – 8251.
[34] D. Wang, X. D. Wang, Y. L. Guo, W. S. Liu, W. W. Qin, *RSC Adv.* **2014**, *4*, 51658 – 51665.
[35] K. Suzuki, L. Malfatti, D. Carboni, D, Loche, M, Casula, A. Moretto, M. Maggini, M. Takahashi, P. Innocenzi, *J. Phys. Chem. C* **2015**, *119*, 2837 – 2843.
[36] Z. Zhang, J. H. Hao, W. S. Yang, B. P. Lu, X. Ke, B. L. Zhang, J. L. Tang, *ACS Appl. Mater. Interfaces* **2013**, *5*, 3809 – 3815.
[37] Y. Tao, E. G. Ju, J. S. Ren, X. G. Qu, *Chem. Commun.* **2014**, *50*, 3030 – 3032.
[38] X. M. Chen, X. T. Tian, B. Y. Su, Z. Y. Huang, X. Chen, M. Oyama, *Dalton Trans.* **2014**, *43*, 7449 – 7454.
[39] Y. W. Zhang, J. Q. Tian, S. Liu, L. Wang, X. Y. Qin, W. B. Lu, G. H. Chang, Y. L. Luo, A. M. Asiri, A. O. Al-Youbi, X. P. Sun, *Analyst* **2012**, *137*, 1325 – 1328.
[40] J. H. Hao, Z. Zhang, W. S. Yang, B. P. Lu, X. Ke, B. L. Zhang, J. L. Tang, *J. Mater. Chem. A* **2013**, *1*, 4352 – 4357.
[41] H. L. Tan, C. J. Ma, L. Gao, Q. Li, Y. H. Song, F. G. Xu, T. Wang, L. Wang, *Chem. Eur. J.* **2014**, *20*, 16377 – 16383.
[42] A. K. Dutta, S. Das, S. Samanta, P. K. Samanta, B. Adhikary, P. Biswas, *Talanta* **2013**, *107*, 361 – 367.

Received: March 13, 2015
Revised: April 16, 2015
Published online on July 20, 2015

© 2015 Wiley-VCH Verlag GmbH & Co. KGaA, Weinheim